Water-in-Oil Microemulsion Synthesis of Platinum−Ruthenium Nanoparticles, Their Characterization and Electrocatalytic Properties

Xin Zhang† and Kwong-Yu Chan*

Department of Chemistry, The University of Hong Kong, Pokfulam Road, Hong Kong SAR, China

Received April 12, 2002. Revised Manuscript Received October 29, 2002

Mixed platinum−ruthenium nanoparticles are prepared by water-in-oil reverse microemulsions of water/Triton X-100/propanol-2/cyclohexane. Nanoparticles formed in the microemulsions are characterized by transmission electron microscopy (TEM), electron diffraction (ED), X-ray diffractometry (XRD), energy-dispersive X-ray analysis (EDX), and X-ray photoelectron spectroscopy (XPS). TEM results show a narrow distribution of Pt−Ru nanoparticles. A homogeneous alloy structure in the bimetallic nanoparticles is indicated by XRD analysis and ED analysis. The composition of the Pt−Ru nanoparticles can be easily controlled by the relative concentration of Pt and Ru in the initial precursor solution. The composition that was in the Pt−Ru nano-alloy is found to be the same as that in the original precursor solution. XPS analysis reveals the presence of Pt and Ru metal as well as some oxide of ruthenium. The effect of precursor concentration on microemulsion drop size was investigated by photo correlation spectroscopy (PCS) measurement. The size of Pt−Ru nanoparticles depends on the concentration of precursor in the aqueous phase. At low precursor concentration, the final particle size is about 2.5 nm and appears to be limited by nucleation. At high precursor concentration, the final particle size is about 4.5 nm and appears to be limited by the collisions and mixing with thousands of hydrazine droplets. The Pt−Ru nanoparticles supported on a carbon electrode possessed high dispersion and high catalytic activity for methanol oxidation at room temperature.

Introduction

The preparation of nanoparticles has received considerable attention in recent decades because nanoparticles possess unique physical and chemical properties.[1,2] Nanosized materials have found promising technological applications in many different areas such as microelectronic devices,[3,4] photocatalysis,[5] electrocatalysis,[6,7] biomedical applications,[8,9] and chemical processes.[10,11] A number of techniques have been used for producing nanoparticles, including vapor phase techniques,[12] sol−gel methods,[13] sputtering[14] and coprecipitation.[15] The synthesis of mixed metal nanoparticles is attracting a lot of recent interest for their catalytic properties. In particular, supported and unsupported Pt−Ru nanoparticles have been investigated for their superior electrocatalytic activity for methanol oxidation and CO tolerance oxidation[16] related to fuel cell applications.

The synthesis of mixed metal nanoparticles is a complex problem because of the composition control in addition to size and size distribution control. Platinum−ruthenium bimetallic catalysts have been prepared by co-impregnation methods[17,18] but without good control of particle size, size distribution, and chemical composition. An alternative method, in which molecular cluster compounds were used as precursors, has been developed.[19,20] The colloidal method to synthesize Pt−Ru nanoparticles through the co-reduction of platinum and ruthenium chlorides has been developed.[21] Nashmer et

* Author for correspondence. Fax: (852) 28571586. E-mail: hrsccky@hku.hk.

† Permanent address: Department of Chemistry, Shantou University, Shantou, China 515063

(1) Service, R. F. *Science* **1996**, *271*, 920.
(2) Siegel, R. W. *Phys. Today* **1993**, *46* (10), 64.
(3) Colvin, V. L.; Schlamp, M. C.; Alivisatos, A. P. *Nature* **1994**, *370*, 354.
(4) Sugimoto, M. *J. Am. Ceram. Soc.* **1999**, *82*, 269.
(5) Hoffman, A. J.; Mills, G.; Yee, H.; Hoffmann, M. R. *J. Phys. Chem.* **1992**, *96*, 5546.
(6) Brus, L. *J. Phys. Chem.* **1986**, *90*, 2555.
(7) Joo, S. H.; Choi, S. J.; Oh, I.; Kwak, J.; Liu, Z.; Terasaki, O.; Ryoo, R.; *Nature* **2001**, *412*, 169.
(8) Hafeli, U.; Schutt, W.; Teller, J.; Zborowski, M. E. *Scientific and Climical Applications of Magnetic Carriers;* Plenum: New York, 1997.
(9) Santra, S.; Wang, K.; Tapec, R. *J. Biomed. Opt.* **2001**, *6* (2), 160.
(10) Khaleel, A.; Li, W. F.; Klabunde, K. J. *Nanostruct. Mater.* **1999**, *12*, 463.
(11) Bach, U.; Lupo, D.; Comte, P.; Moser, J. E. *Nature* **1998**, *395*, 583.
(12) Siegel, R. W. *J. Mater. Rev.* **1998**, *3*, 1367.
(13) Fegley, B. J.; White, P.; Bowen, H. K. *Am. Ceram Soc. Bull.* **1985**, *64*, 1115.
(14) Fayet, P.; Woste, L. Z. *Phys. D.* **1986**, 3, 177.
(15) Jang, Z. X.; Sorensen, C. M.; Klabunde, K. J.; Hadjipanayis, G. C. *J. Colloid Interface Sci.* **1991**, *146*, 38.
(16) (a)Iwasita, T.; Nart, F. C.; Vielstich, W. *Ber. Bunsen-Ges. Phys. Chem.* **1990**, *94*, 1030. (b) Ross, P. N. *Electrochim. Acta* **1991**, *36*, 2053. (c) Hamnett, A. *Catal. Today* **1997**, *38*, 445. (d) Hogarth, M. P.; Hards, G. A. *Platinum Metals Rev.* **1996**, *40*, 150.
(17) Watanab, M.; Uchina, M.; Motoo, S. *J. Electroanal. Chem.* **1987**, *229*, 395.
(18) Alerasool, S.; Gonzlez, R. D. *J. Catal.* **1990**, *124*, 204.
(19) Basset, J. M.; Candy, J. P.; Chopin, A.; Nedez, C.; Quignard, F.; Santini, C. C.; A. Jheolier, A. *Mater. Chem. Phys.* **1991**, *29*, 5.
(20) Ichikawa, M. *Adv. Catal.* **1992**, *38*, 283.

10.1021/cm0203868 CCC: $25.00
Published on Web 12/18/2002

Table 1. Compositions of the Microemulsion System Used for the Synthesis of Pt−Ru Nanoparticles

	microemulsion I	microemulsion II	volume	vol %
aqueous phase	20 mM H_2PtCl_6 + 20 mM $RuCl_3$	2 M hydrazine	1.5 mL	15
surfactant	TritonX-100	TritonX-100	1 mL	10
cosurfactant	propanol-2	propanol-2	4 mL	40
oil phase	cyclohexane	cyclohexane	3.5 mL	35

al. deposited an organometallic $PtRu_5C(CO)_{16}$ cluster onto carbon black and decomposed it by a high-temperature treatment.[22] More recently, Boxhall et al. reported the synthesis of a Pt_1Ru_1/carbon nanocomposite using microwave irradiation.[23]

The interest of preparing nanoparticles using microemulsions has increased since Boutonnet et al.[24] successfully synthesized platinum nanoparticles by using water/oil (w/o) microemulsions. The microemulsion technique has been widely used to prepare nanoparticles of metal,[24,25] metal sulfides,[26] and metal halides.[27] The preparation of bimetallic nanoparticles has started to appear: e.g., Cu/Au,[28] Pd/Pt,[29,30] Au/Pt,[31] Au/Pd,[32] and Pt/Co.[33] Despite its importance for the electrocatalysis of fuel cell reactions, the Pt−Ru nanoparticles prepared by the w/o microemulsion has not been reported.

In this paper, we report the synthesis of bimetallic Pt−Ru nanoparticles using a water-in-oil reverse microemulsion of water/Triton X-100/propanol-2/cyclohexane. The nanoparticles formed were characterized by transmission electron microscopy(TEM), electron diffraction (ED), X-ray diffractometry (XRD), X-ray photoelectron spectroscopy(XPS), and energy dispersive X-ray analysis (EDX). The effect of aqueous precursor concentration on ultimate particle size is discussed and the performance of the prepared Pt−Ru nanoparticles as electrocatalysts for methanol oxidation are reported.

Experimental Section

A nonionic surfactant Triton X-100 (*t*-octyphenoxypolyethoxyethanal) from Sigma Chemical Co. was used as received. Hydrazine hydrate, propanol-2, and cyclohexane (C_6H_{12}) were from BDH Chemical Ltd. The platinum source was dihydrogen hexachloroplatinate (IV) hydrate($H_2PtCl_6{\cdot}xH_2O$) from Chempure Ltd. The ruthenium source was ruthenium(III) chloride from BDH Chemicals Ltd. Deionized water (18.2 M) was produced by a Milli-Q ultrapure system of Millipore Ltd., USA. The preparation of Pt−Ru nanoparticles was by a two-emulsion technique.[34−35] The microemulsion system used in this study consisted of Triton X-100 as a surfactant, propanol-2 as a cosurfactant, cyclohexane as the continuous oil phase, and either the Pt−Ru precursor solution or hydrazine solution as the dispersed aqueous phase. The aqueous phases in the two microemulsion systems have the same volume fraction but with different compositions as indicated in Table 1. The aqueous phase in microemulsion II contained hydrazine solution as the reducing agent. The amount of hydrazine was in stoichiometric excess compared with the equal volume of Pt−Ru precursor solution in microemulsion I. The two microemulsions were prepared separately by mixing (by volume) 10% surfactant, 35% cyclohaxane, 40% propanol-2, and 15% of the aqueous phase. A small amount of additional propanol-2 was then titrated slowly into each of the microemulsion systems with stirring until the microemulsion system turned transparent. The two stable microemulsions were then mixed with a stirrer. Platinum−ruthenium nanoparticles were formed upon contact between the precursor containing droplets and the hydrazine containing droplets. The reduction reactions could be expressed as

$$H_2PtCl_6 + N_2H_4 \rightarrow Pt^0 + 6\ HCl + N_2 \qquad (1)$$

and

$$4\ RuCl_3 + 3\ N_2H_4 \rightarrow 4\ Ru^0 + 3\ N_2 + 12\ HCl \qquad (2)$$

The Pt−Ru nanoparticles were characterized by a JEOL 2000FX transmission electron microscope. The TEM sample was prepared by placing a 100-μL drop of Pt−Ru nanoparticle solution onto a carbon-coated copper TEM grid, which was left to dry in a desiccator. Single-particle resolution energy dispersion X-ray analysis (TEM-EDX) was used to examine the individual nanoparticle compositions using a Philips CM 120 transmission electron microscope (TEM) equipped with an EDX detection unit (model R-TEM, CM-12(TWIN) 139-5 system). X-ray diffraction (XRD) measurements were performed on a (Siemens, D-5000) X-ray diffractometer using Cu K radiation (λ = 0.1542 nm). The sample for XRD analysis was prepared by adding the Vulcan 72 high-surface-area carbon into microemulsions of Pt−Ru nanoparticles to adsorb the nanoparticles. The Pt−Ru nanoparticles loaded carbon were then heated at 500 °C in a nitrogen atmosphere, for better characterization of XRD. XPS spectra were recorded by a Phi Quantum 2000 XPS system (Physical Electronics, Inc.) using AlK_α radiation at a base pressure below 5×10^{-9} Torr. The preparation of the sample for XPS analysis is the same as that of XRD. Nonlinear least-squares curve-fitting was performed using the Phi Multipack software (Physical Electronics, Inc.). Photon correlation spectroscopy (PCS) measurements were carried out at room temperature (25 °C) with a Zelasizer 3000 HS equipment (Malvern Instruments Ltd. UK). The wavelength of the internal laser was 633 nm and the selected measurement scattering angle was 90 degrees.

Two microemulsion systems were thoroughly mixed to achieve reduction of Pt/Ru. A carbon paper circular electrode

(21) (a) Schmdt, T. J.; Noeske, M.; Gasteigar, H. A.; Behm, R. J.; Britz, P.; Brijouz, W.; Bönnemann, H. *Langmuir* **1997**, *13*, 2591. (b) Bönnemann, H.; Brinkmann, R.; Britz, P.; Endruschat, U.; Mortel, R.; Paulus, U. A.; Feldmeyer, G. J.; Schmidt, T. J. J. *New Mater. Electrochem. Syst.* **2000**, *3*, 199. (c) Liu, M.; Yu, W.; Liu, H.; Zheng, J. *J. Colloid Interface Sci.* **1999**, *214*, 231. (d) Vogel, W.; Britz, P.; Bonnemann, H.; Rothe, J.; Hormes, J. *J. Phys. Chem. B* **1997**, *101*, 11029.

(22) (a) Nashmer, M. S.; Frenkel, A. I.; Adler, D. L.; Shapley, J. R.; Nuzzo, R. G. *J. Am. Chem. Soc.* **1997**, *119*, 7760. (b) Nashmer, M. S.; Frenkel, A. I.; Somerville, D.; Hills, C. W.; Shapley, J. R.; Nuzzo, R. G. *J. Am. Chem. Soc.* **1998**, *120*, 8093.

(23) Boxall, D. L.; Deluga, G. A.; Kenik, E. A.; King, W. D.; Lukehart, C. M. *Chem. Mater.* **2001**, *13*, 891−900.

(24) Boutonnet, M.; Kizting, J.; Stenius, P. *Colloids Surf.* **1982**, *5* (3), 209.

(25) Chen, D. H.; Wu, S. H. *Chem. Mater.* **2000**, *12*, 1354.

(26) Kortan, A. R.; Hull, R.; Opila, R. L.; Bawendi, M, G.; Steigerwald, M. L.; Carroll, P. J.; Brus, L. E. *J. Am. Chem. Soc.* **1990**, *112*, 1327.

(27) Pillai, V.; Kumar, P.; Multani, M. S.; Shah, D. O. *Colloids Surf. A* **1993**, *80*, 69.

(28) Sangregorio, C.; Galeotti, M.; Bardi, U.; Baglioni, P. M. *Langmuir* **1996**, *12*, 5800.

(29) Touroude, R.; Girard, P.; Maire, G.; Kizling, J.; Boutonnet-Kizling, M.; Stenius, P. *Colloids Surf.* **1992**, *67*, 9.

(30) Wu, M. L.; Chen, D. H.; Huang, T. C. *J. Colloid Interface Sci.* **2001**, *243*, 102.

(31) Wu, M. L.; Chen, D. H.; Huang, T. C. *Chem. Mater.* **2001**, *13*, 599.

(32) Wu, M.-L.; Chen, D.-H.; Huang, T.-C. *Langmuir* **2001**, *17*, 3877.

(33) (a) Zhang, X.; Chan, K. Y. *J. Mater. Chem.* **2002**, *12*, 1203. (b) Chi, N.; Chan, K. Y.; Phillips, D. L. *Catal. Lett.* **2001**, *71*, 21.

(34) J. Wang, E, L. S., Ng, S. C.; Chew, C. H.; Gan, L. M. *Mater. Lett.* **1997**, *30*, 119.

(35) Lee, M. H.; Tai, C. Y.; Lu, C. H. *J. Eur. Ceram. Soc.* **1999**, *19*, 2593.

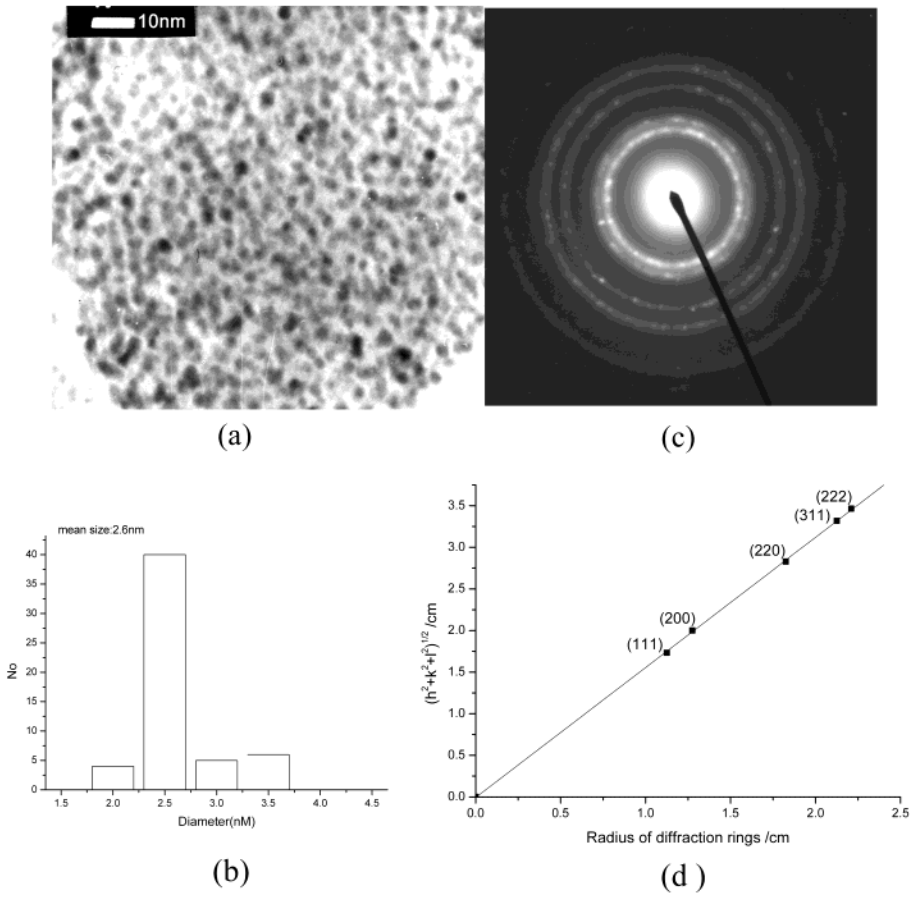

Figure 1. (a) Transmission electron micrograph of Pt−Ru nanoparticles prepared by the w/o microemulsion method. (b) Pt−Ru nanoparticle size distribution histogram. (c) Electron diffraction pattern of a region of the same sample. (d) Electron diffraction rings indexed in *hkl* order.

with 9 mm diameter (area 0.64 cm^2) was used as substrate for the Pt−Ru nanoparticle catalysts. For the electrode preparation, a suspension of 0.87 mg Pt/mL microemulsion was pipetted onto the surface of a ELAT carbon cloth electrode supplied by E-TEK Inc., MA. The loading of platinum was calculated by the amount of solution added onto a known surface area of carbon electrode, assuming complete and uniform adsorption. After evaporation of the solvent at 60 °C in an oven, the carbon electrode was immersed several times in ethanol and then dried in air. When immersed into an aqueous electrolyte solution, the electrodes thus prepared did not have the nanoparticles redissolved and the electrolyte solution remained colorless throughout. For the TEM analysis, the Pt−Ru loaded carbon was carefully stripped from the carbon paper and suspended in ethanol before dropping it onto a TEM grid. All electrochemical measurements were taken in a three-compartment electrochemical cell. The potentiostats used include the VOLTALAB 40 of Radiometer and BAS LG-50 of Bioanalytical Systems Inc. USA. A Ag/AgCl electrode was used as the reference electrode for the methanol oxidation experiments in acid solution.

Results and Discussion

Chacterization of Pt−Ru Nanoparticles. The platinum−ruthenium nanoparticles form readily at room temperature upon mixing of the two microemulsion systems. The nanoparticles suspended in solution are analyzed for their size distribution, crystal structure, and chemical compositions by depositing and letting them dry on a TEM grid. Figure 1(a) shows a typical TEM image of the Pt−Ru nanoparticles deposited on the TEM grid. The precursor concentration is 20 mM H_2PtCl_6 plus 20 mM $RuCl_3$. A histogram of particle diameters constructed in Figure 1(b) indicates an average diameter of 2.6 nm with a standard deviation of 0.2 nm. The Pt−Ru nanoparticles show some degree of crystallinity by electron diffraction with the TEM equipment. Figure 1(c) shows the electron diffraction pattern obtained from a selected area of Figure 1(a). The bright rings with occasional bright spots are due to the presence of polycrystals. Pure platinum has a face-centered cubic lattice structure whereas pure ruthenium has a hexagonal structure, as is well-known.[36] However, in this electron diffraction pattern of the Pt−Ru bimetallic catalyst, only diffractions from the face-centered cubic (fcc) lattice structure appear. This is due to the formation of a Pt−Ru binary alloy with the fcc structure. A plot of the root of the sum of squares of the lattice coordinates versus the radius of the concentric rings was constructed and is shown in Figure 1(d). A linear relationship can be established with the lattices (111), (200), (220), (311), and (222). This indicates a face centered cubic (fcc) structure with a calculated lattice cell constant of 3.862 Å. This lattice constant is between those of platinum and ruthenium and is in agreement with that of a Pt_1Ru_1 alloy.[36−37] The TEM electron

(36) (a) Ageev, N. V.; Kuznetsov, V. G.; *Izvest. Akad. Nauk, S. S. S. R. (Khim)*, **1937**, 753. (b) Hutchinson, J. M., Jr. *Platinum Met. Rev.* **1972**, *16*, 88−90. (c) Bommarius, A. S.; Holzarth, J. F.; Wang, D. I. C.; Hatton, T. A. *J. Phys. Chem*. **1990**, *94*, 7232.

(37) Radmilovic, V.; Gasteiger, H. A.; Ross, P. N., Jr. *J. Catal.* **1995**, *154*, 98.

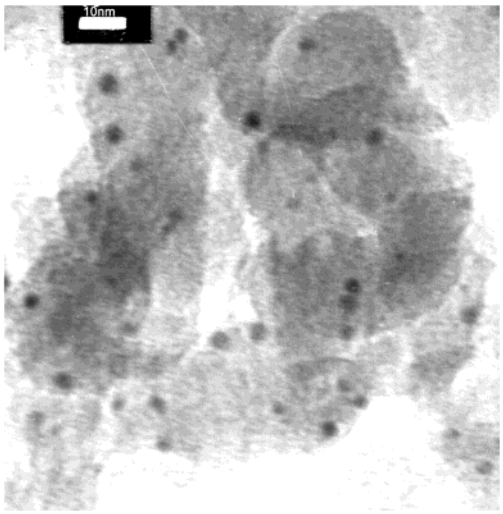

Figure 2. Bright-field TEM micrograph of the Pt−Ru nanoparticles supported on Vulcan carbon 72.

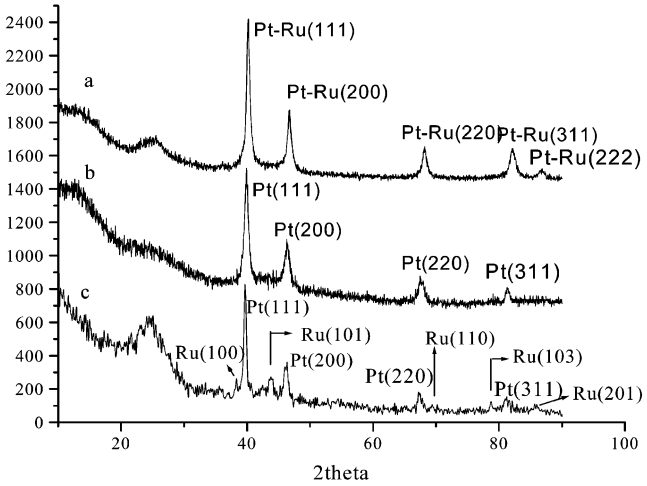

Figure 3. X-ray diffraction patterns of metallic nanoparticles supported on carbon: (a) Pt−Ru/Vulcan 72 carbon; (b) Pt/Vulcan 72 carbon; (c) physically mixed Pt/C and Ru/C powders in 1:1 ratio.

diffraction data indicate the interpenetration of the Ru into a Pt lattice, leading to reduced *d* spacing and lattice constant.

For fuel cells and other catalytic applications, metallic nanopartices are usually supported on a high-surface-area substrate such as activated carbon. The Pt−Ru nanoparticles supported on Vulcan 72 carbon were also characterized. Figure 2 shows a TEM micrograph of Pt−Ru nanoparticles adsorbed onto high-surface-area Vulcan 72 carbon and after heat treatment in an inert atmosphere. The heat treatment at 500 °C in nitrogen allows for a better contrast in the TEM image. The size of the Pt−Ru nanoparticles increases slightly and the distribution broadens upon annealing. X-ray diffraction (XRD) was performed for the carbon supported platinum−ruthenium nanoparticles to analyze the structure of the particles. Although XRD results can be obtained without heat treatment, the annealing enhances the crystallinity and the XRD peaks. The XRD results are displayed in Figure 3 for 2θ angle values of 10−90°. For comparison, the XRD pattern of the pure Pt fcc structure is also shown in Figure 3. Curve c in Figure 3 shows the XRD pattern of a physical mixture of pure Pt in carbon and pure Ru in carbon. Small peaks appear in curve c, corresponding to the ⟨100⟩, ⟨101⟩, ⟨110⟩, ⟨103⟩, and ⟨201⟩ diffraction peaks in the hexagonal structure (hcp) of pure ruthenium. The diffraction peaks in the Pt−Ru catalyst of curve a matches the ⟨111⟩, ⟨200⟩, ⟨220⟩, and ⟨311⟩ characteristics of a platinum fcc structure but slightly shifted to higher 2θ values. There were also no observable lines in the XRD spectra corresponding to those of pure ruthenium. If the homogeneous solid solution of Pt−Ru was not formed, the XRD spectra of pure Ru in hcp structure would be observed at the same time as in curve (c). The shift in 2θ in curve a corresponds to a decrease in the lattice constant due to the incorporation of Ru atoms. This is in agreement with the electron diffraction result shown earlier and provides evidence for the presence of a well-mixed Pt−Ru alloy. As in the ED results, the Pt−Ru nanoparticle alloys are not completely crystalline. The diffraction peak positions of the ⟨111⟩, ⟨200⟩, ⟨220⟩, ⟨311⟩, and ⟨222⟩ planes are at 2θ of 40.39°, 46.92°, 68.27°, 82.21°, and 86.74°, and are related to *d* spacing of 2.2312 Å, 1.935 Å, 1.375 Å, 1.172 Å, and 1.122 Å, respectively. The lattice constant of 3.862 Å can be calculated from the ⟨111⟩ plane. This lattice suggests a composition of 50% Pt and 50% Ru according to a linear relationship between lattice constant and composition. These results are in very good agreement with the ED results in the TEM analyses. Energy-dispersive X-ray analyses (TEM-EDX) are also conducted by focusing the electron beam on several different selected individual Pt−Ru nanoparticles on each sample of the unsupported Pt−Ru nanoparticles. A typical EDX spectrum of the Pt−Ru nanoparticles is shown in Figure 4. The average composition of the irradiated nanoparticle was in the atom ratio of Pt/Ru = 1.07:1. The compositions of Pt and Ru in different individual particles are in close agreement with little deviation. This shows little inhomogeneity of composition in the nanoparticles and the formation of the Pt−Ru bimetallic nanoparticle alloy. The appearance of Cu peaks in Figure 4 is due to the TEM copper grid supporting the sample.

Although the TEM, XRD, and EDX results are in agreement and show the presence of 1:1 Pt−Ru alloy state in the nanoparticles, it may be possible that oxides are present in addition to alloy crystals. To investigate the oxidation states of Pt and Ru in the nanoparticles, X-ray photoelectron spectroscopy (XPS) analyses are performed on the Pt−Ru nanoparticles/C catalysts. Figure 5(a) shows the region for Pt4f in the XPS spectrum of the Pt−Ru nanoparticles. The spectrum can be fit by two pairs of overlapping Lorentzian curves. The $Pt4f_{7/2}$ and $Pt4f_{5/2}$ lines appearing at 71.30 eV (peak 1) and 74.57 eV (peak 3) are attributed to metallic Pt^0. The second pair appearing at 72.49 eV (peak 2) and 75.88 eV (peak 4) can be assigned to Pt^{II} in PtO and $Pt(OH)_2$.[38] The relative heights indicate that metallic Pt^0 is the predominant species. Considering the Ru 3d signal overlaps with the C1S signal of the carbon support, the Ru $3p_{3/2}$ signal was analyzed and the corresponding XPS region is shown in Figure 5(b). The Ru $3p_{3/2}$ spectrum gives three components with bonding energies of 461.32, 463.41, and 465.72 eV. The peaks can be assigned as

(38) Baer, Y.; Heden, P. F.; Hedeman, J.; Klasson, M.; Nording, C.; Siegbahn, K. *Phys. Scr.* **1970**, *1*, 55.

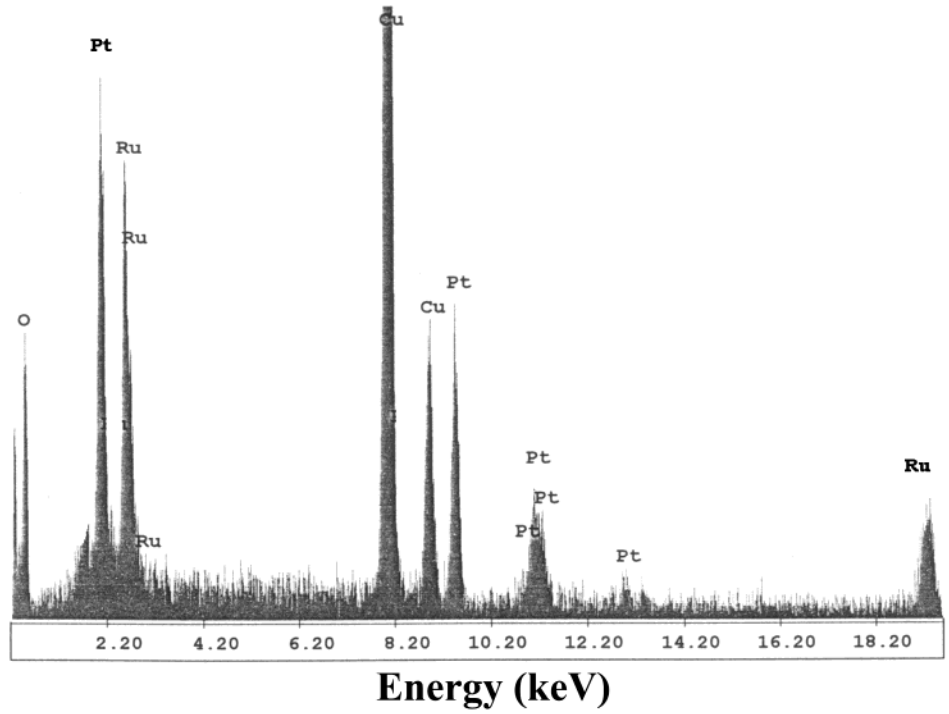

Figure 4. Broad area TEM-EDX spectra of the unsupported Pt−Ru nanoparticles. The copper lines are due to TEM grid.

461.32 eV (peak 1) to Ru^0 metal, 463.41 eV (peak 2) to Ru^{IV} (e.g. RuO_2), and the 465.72 eV (peak 3) to the higher oxidation state of Ru^{VI} in RuO_3.[39] The XPS results indicate some presence of Ru oxides and metal on the surface of the nanoparticles. The surface of the nanoparticles is composed mainly of Ru oxides and Pt^0 metal as reported previously.[40] It is likely that Pt−Ru/Vulcan carbon nanocomposites undergo significant oxidation of Ru upon exposure to ambient air to form hydrated ruthenium oxide. The presence of oxygen species in the Ru oxide may give the catalytic property required for CO oxidation. The bimetallic nanoparticle provides bifunctional catalytic character for important fuel cell reactions such as direct oxidation of methanol.[41]

Composition Control. The main attractive features of the two-step microemulsion reduction technique for preparing mixed metal nanoparticles are the ease and accuracy of composition control. The reduction reaction occurs in a confined reaction zone within the microemulsions. The extent and uniformity of the reduction reaction can be controlled. The final nanoparticles should follow the metal composition in the precursor solution, without losing control of the particle size. The preparation of nanoparticles with adsorption into a carbon support prevents loss of size and composition control. The optimization of composition and size of mixed metal at the nanometer level is the main subject of electrocatalysis for fuel cell applications. We performed preparations of various Pt−Ru nanoparticles by changing the initial composition of precursor solution. The volume fractions of aqueous phase, surfactant, cosurfactant, and oil phase are the same as in Table 1.

Table 2. EDX Results of Pt−Ru Nanoparticle and the Corresponding Compositions of Precursor

initial atomic composition Pt/Ru	structure of nanoparticles	atomic composition in nanoparticle Pt/Ru
4:1	fcc	4.7:1
3:1	fcc	2.91:1
2:1	fcc	2.07:1
1:1	fcc	1.07:1
0.5:1	fcc	0.535:1

The concentration of the H_2PtCl_6 is kept at 20 mM but the $RuCl_3$ concentration varies correspondingly. The characterization results show that the composition of bimetallic nanoparticles followed closely that of the initial metal salt solution. Table 2 shows the SEM-EDX results of several bimetallic Pt−Ru nanoparticles and the composition of their initial precursor solutions. The SEM-EDX results analyses are close to that of TEM-EDX but are over many particles in a larger area. The various compositions of the resulting Pt−Ru nanoparticles are in agreement with the composition of the initial precursor solution.

Effect of Precursor Concentration on Particle Size. In the two-step reverse microemulsion technique, the control of particle size depends on many parameters. The water/surfactant ratio, cosurfactant/water ratio, and concentration of aqueous phases are some of the parameters to be optimized. Table 1 represents a set of feasible experimental conditions for the preparation of Pt−Ru nanoparticles. Changes in the concentrations of the Pt−Ru aqueous phase are required to achieve different compositions of nanoparticles as illustrated in Table 2. We therefore studied the effect of precursor concentration on the size of the nanoparticles formed. Table 3 shows the various concentrations of Pt and Ru salt in the precursor phase used in such a study. The volume fractions and other parameters are the same as those in Table 1. The resulting diameters of the unsupported Pt−Ru nanoparticle from TEM analyses are also

(39) Arico, A. S.; Creti, P.; Kim, H.; Mantegna, R.; Giordano, N.; Antonucci, V. *J. Electrochem. Soc.* **1996**, *143* (12), 3950.
(40) Rolison, P. R.; Hagans, P L.; Swider, K. E. *Langmuir* **1999**, 15, 774.
(41) Lin, S. D.; Hsiao, T. C.; Chang, J. R.; Lin, A. S. *J. Phys. Chem.* **1999**, *103*, 97.

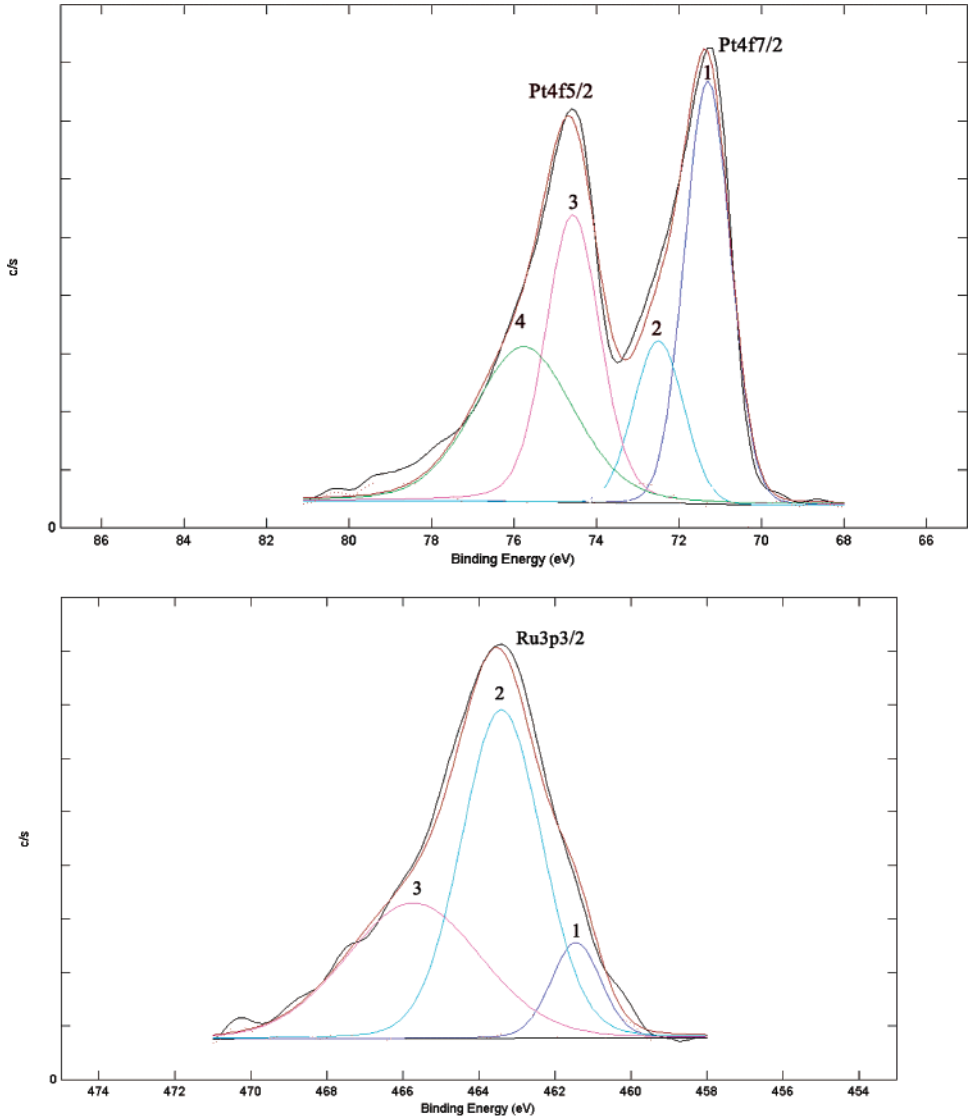

Figure 5. XPS spectrum of the Pt−Ru nanoparticles/Vulcan carbon: (a) Pt4f, peak 1 shows the $Pt4f_{7/2}$ (71.3ev) line of metal Pt^0; peak 2 shows the $Pt4f_{7/2}$(72.49ev) line of metal Pt^{II}; peak 3 shows the $Pt4f_{5/2}$(74.57ev) line of metal Pt^0; peak 4 shows the Pt $4f_{5/2}$ (75.88ev) line of metal Pt^{II}; (b) $Ru3p_{3/2}$.

Table 3. Variations of TEM Diameters and Microemulsion Parameters with Concentration of Pt−Ru Precursor Solution[a]

Pt−Ru precursor solution concn. (mM)	particle diam. from TEM (nm)	diam. of Pt−Ru microemulsion droplet determined by PCS (nm)	Pt−Ru particle diam. if made from one microemulsion droplet (nm)	number of hydrazine droplets to completely react with one precursor droplet	number of precursor droplets in 1 mL of microemulsion	hydrazine droplets per Pt−Ru droplets	overall stoich. excess of hydrazine
2	2.5 ± 0.2	26.2 ± 2.6	0.855	14.7	15.9×10^{15}	4.2×10^3	571
6	2.6 ± 0.3	27.6 ± 2.8	1.30	51.7	13.6×10^{15}	4.9×10^3	190
10	2.5 ± 0.2	26 ± 2.7	1.45	71.7	16.3×10^{15}	4.1×10^3	114
20	2.6 ± 0.2	28.7 ± 2.9	2.02	0.19×10^3	12.1×10^{15}	5.5×10^3	57.1
40	4.0 ± 0.5	40.7 ± 3.1	3.61	1.1×10^3	4.25×10^{15}	15.8×10^3	28.5
60	4.5 ± 1.0	55.9 ± 4.5	5.67	4.3×10^3	1.64×10^{15}	40.9×10^3	19.0
100	4.6 ± 1.1	83.3 ± 5.2	10.02	23.6×10^3	0.49×10^{15}	136×10^3	11.4

[a] 2 mM Solution means 2 mM H_2PtCl_6 + 2 mM $RuCl_3$. Diameter of hydrazine microemulsion droplet is 1.62 nm as measured by PCS, and corresponding concentration is 6.7×10^{19} per mL.

shown in Table 3 and Figure 6. Figure 6 shows two plateaus of particle sizes 2.5 and 4.5 nm corresponding to low and high metal salt concentrations, respectively. The particle size was around 2.5 nm and unaffected by the Pt−Ru concentration when it was below 20 mM. When the Pt−Ru concentration was above 20 mM, the size of Pt−Ru nanoparticles increased with the metal salt concentration until 60 mM, beyond which the average nanoparticle size remained at 4.5 nm. This size dependence on concentration of precursor was similar to that reported in ref 25 for nickel nanoparticles prepared from $NiCl_2$ and hydrazine with a cationic surfactant.

Understandably, the steps of the nanoparticle formation process are (1) meeting of the reducing agent with the precursor, (2) nucleation of a nano metal particle,

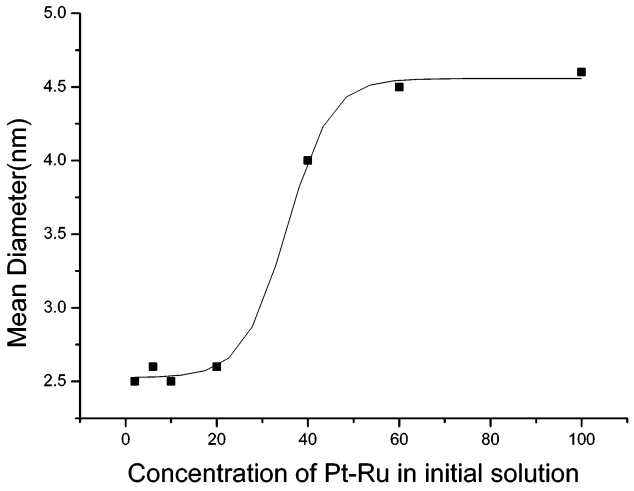

Figure 6. Relation between the mean diameter of Pt−Ru nanoparticles and metal ion concentration in precursor.

and (3) growth of the metal nucleus. The first step would be the most critical because the amount of reduced material present and the local environment will determine how step (2) or step (3) will proceed. The presence of surfactant confines the reduction process that starts when the reducing agent and the precursor meet after merging of the microemulsion droplets. The size and number of the microemulsion droplets, and the probability and frequency of merging of the two kinds of microemulsion droplets are important factors to consider. A photon correlation spectroscopy (PCS) particle sizer was used to determine the microemulsion droplet size. Table 3 and Figure 7 show the PCS-determined hydrodynamic diameters of the hydrazine microemulsion droplets and the Pt−Ru droplets as a function of precursor concentration. A narrow distribution of droplet sizes was found in each of the microemulsion systems. The hydrodynamic diameter of the hydrazine microemulsion droplets was 1.62 nm, whereas that of Pt−Ru complex varies from 26.2 at 2 mM Pt−Ru to 83.3 nm at 100 mM Pt−Ru. Although the total amount of hydrazine present is in stoichiometric excess, in the local microemulsion environment, several hydrazine droplets are needed to completely reduce a single Pt and Ru ion-containing droplet. As tabulated in Table 3, this number grows rapidly with precursor concentration because the size of the Pt and Ru ion-containing droplet increases with concentration in addition to the increasing stoichiometric demand. The number of Pt−Ru droplets decreases with concentration because the droplet size increases. In these calculations, it has been assumed that the diameter of the aqueous part of the microemulsion is the same as the PCS hydrodynamic diameter, and the length of the surfactant has been ignored. It was observed that with the addition of a cosurfactant, the surfactant molecule does not extend into the oil phase.[42] We have compared the hydrodynamic diameter of surfactant plus oil phase with and without the presence of a cosurfactant. The PCS-measured diameter of the surfactant micelle decreases by approximately the length of the surfactant when a cosurfactant is added.

(42) Attwood, D. *Colloidal Drug Delivery Systems*; Dekker: New York, 1994; p. 31. (b) Warisnoicharoen, W.; Lansley, A. B.; Lawrence, M. J. *AAPS Pharm. Sci.* **2000**, *2*, 429.

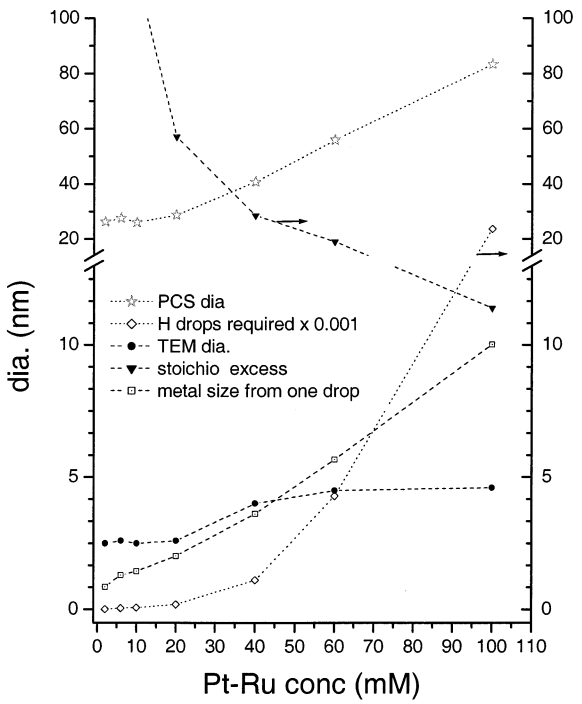

Figure 7. Variations of parameters related to microemulsion droplet and Pt−Ru concentration in precursor: ●, TEM diam.; ☆, Pt−Ru droplet diam. measured by PCS; □, equivalent nanoparticle diam. produced by a single Pt−Ru droplet; ♢, 0.001 × the number of hydrazine droplets required to completely reduce a single Pt−Ru droplet; and ▼, stoichiometric excess of the total amount of hydrazine in the two microemulsion system.

If the Pt−Ru alloy nucleated and stopped growing with the entrance of a single hydrazine droplet, then its size should be limited by the stoichiometric amount of Pt−Ru alloy formed by a hydrazine droplet. This size is calculated to be 0.349 nm and is much below that observed with TEM. The observed size is not limited by the TEM resolution, which is below 1 nm. It can be concluded that collisions with multiple hydrazine emulsion droplets are required to form the nanoparticles observed by TEM. On the other hand, the nanoparticle could be formed from a single Pt−Ru emulsion droplet, whose size increases with precursor concentration. The calculated Pt−Ru sizes are tabulated in Table 3. This monotonic size increase, however, does not agree with the trend of the TEM results. At low precursor concentrations, several Pt−Ru droplets are required to come together to form the size of nanoparticle observed by TEM. On the other hand, for concentrations at and above 40 mM, one Pt−Ru droplet would form many nanoparticles.

As discussed by Chen and Wu[25] in their preparations of Ni nanoparticles with the two step w/o microemulsion method, the nanoparticle size is limited by the nucleation process at low precursor concentrations. From our results, it is very probable that a minimum size of 2.5 nm was required to overcome the surface energy during nucleation of a Pt−Ru nanoparticle. For precursor concentrations below 20 mM, several Pt−Ru droplets are required to form a nucleus, and collisions with a stoichiometric number of hydrazine droplets are also required. The need of multiple collision was also proposed in reference 43. Beyond 20 mM, a single precursor

droplet contains Pt−Ru beyond the nucleation limit, and growth can occur upon the entrance of hydrazine droplets. It should be emphasized that the probability of collision among Pt−Ru-containing droplets is very low because at 40 mM, they are outnumbered by the hydrazine droplets by a factor of $>10^4$. It is also known that mobility of a larger colloid decreases with size. The ratio of the number of hydrazine droplets to Pt−Ru droplets is also tabulated in Table 3.

It is more difficult to explain the flattening of the curve in Figure 6 at high precursor concentrations. It is unclear from direct experimental observations what limits the growth of the nanoparticles. The analyses of microemulsion droplet size and their number density in Table 3 offers certain probable explanations. As the increase of precursor concentration is coupled with the increase of the droplet size, the number of hydrazine droplets required to completely reduce a single Pt−Ru droplet increases very rapidly to $>10^5$ at 100 mM. The complete growth to the maximum alloy size would be a very long process and during this time other nuclei would have formed to deplete the supply of Pt−Ru precursor. Although still in stoichiometric excess, the availability of hydrazine droplets also decreases quickly with increasing Pt−Ru precursor concentration. This also places a limit for further growth of particle size. Because of the time required to grow a large particle and the possibility of forming multiple nuclei in a big and concentrated PtRu droplet, it is also observed that the size distribution broadens at higher precursor concentrations. The control of size distribution can be achieved better by using low metal concentration or decreasing the size of the microemulsion droplets containing the metal complex by improving surfactant and microemulation parameters. Other factors that influence the nanoparticle size, such as intermicellar interactions and the intermicellar exchange rate have also been pointed out.[44]

Electrochemical Investigation. Platinum−ruthenium is considered the best catalyst for direct methanol fuel cell and carbon monoxide tolerant anode oxidation. To investigate the performance of Pt−Ru nanoparticles prepared by microemulsion preparation methods, we tested the electrocatalytic activity for methanol oxidation in acidic electrolyte. Figure 8 (a) shows the step current (chronopotentiometry) results for the room-temperature oxidation of methanol on the Pt−Ru nanoparticles/carbon paper electrode prepared by microemulsion with three different Pt loadings. The precursor concentration is 20 mM H_2PtCl_6 and 20 mM $RuCl_3$. A lower polarization of methanol oxidation can be observed for all three electrodes at different Pt loadings. The electrode prepared from the higher Pt−Ru nanoparticle loading can maintain higher current densities, whereas more effective utilization of catalyst at a lower loading electrode was observed. Figure 8(b) shows step-current results for the Pt−Ru nanoparticles/carbon electrode, pure Pt nanoparticles/carbon, and pure Ru nanoparticles/carbon electrode. The Pt−Ru nanoparticles/carbon electrode gives the highest activity and

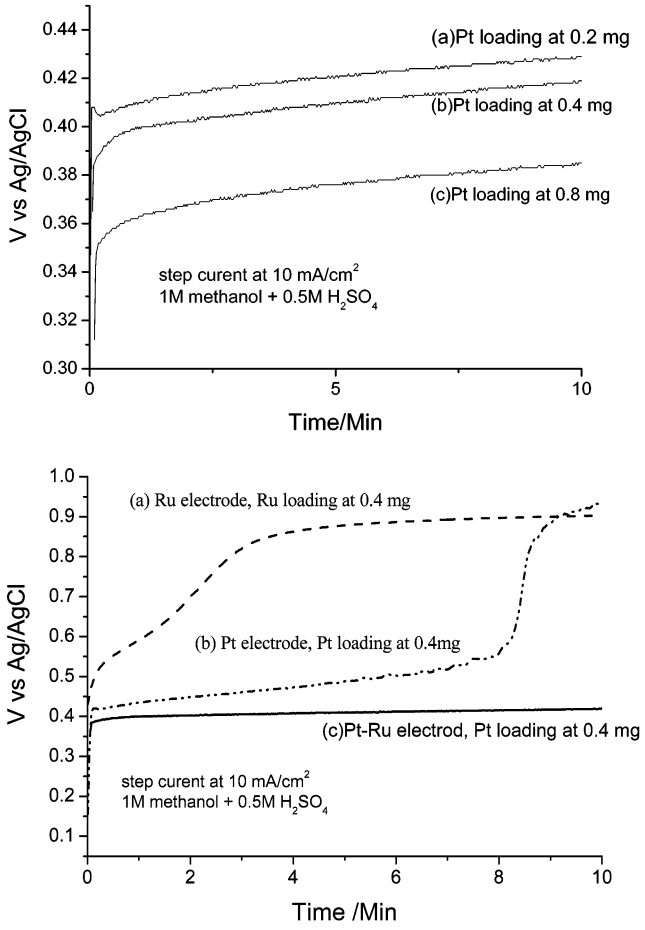

Figure 8. Chronopotentiograms of methanol oxidation at 10 mA/cm^2 in 1 M methanol + 0.5 M H_2SO_4 at room temperature at different Pt loadings. The nanoparticles are prepared from precursor solution with 20 mM H_2PtCl_6 and 20 mM $RuCl_3$: (a) Pt−Ru nanoparticle loaded electrode; (b) different electrodes with separate loadings of Pt nanoparticles, Ru nanoparticles, and Pt−Ru nanoparticles at the same loading of 0.4 mg/cm^2 of Pt or Ru.

longest stability. The pure Ru nanoparticle/carbon electrode has little activity for the electro-oxidation of methanol in room temperature. These results are in agreement with those reported in the literature.[45] Figure 9 shows the same result as Figure 8(a) at the same loading but for a different particle size. The carbon paper electrode loaded with the small particle size alloy has higher performance than that loaded with the large particle size alloy. Figure 10 shows cyclic voltammograms of methanol oxidation on Pt−Ru nanoparticles/carbon paper electrode in 0.5 M H_2SO_4 solution containing 1 M CH_3OH at room temperature. The onset of methanol oxidation is around 0.2 V vs Ag/AgCl and a large methanol oxidation peak was observed at 0.55 V vs Ag/AgCl. The potential of this methanol oxidation peak was low compared to that on a pure Pt electrode. The peak observed on the reverse scan at 0.341 V vs Ag/AgCl was due to the reactivation of oxidized Pt-oxide.

The high catalytic activity of the Pt−Ru nanoparticles/carbon paper electrode at room temperature is due to the high surface area of the nanoparticles, their high

(43) Hanna, H. I.; Rahul, B.; Anders, P.; Magnus, S.; Christer, S.; Krister, H.; Dinesh, O. S. *J. Colloid Interface Sci.* **2001**, *241*, 104.

(44) Vincenzo, T. L. In *Nano-Surface Chemistry;* Rosoff, M., Ed.; Marcel Dekker: New York, 2001; p. 492.

(45) (a) Gasteiger, H. A.; Markovic, N.; PRoss, P.N., Jr.; Cairns, E. J. *J. Phys. Chem.* **1993**, *97*, 12020. (b) Gasteiger, H. A.; Markovic, N.; Ross, P. N., Jr.; Cairns, E. J. *J. Electrochem. Soc.* **1994**, *141* (7), 1795.

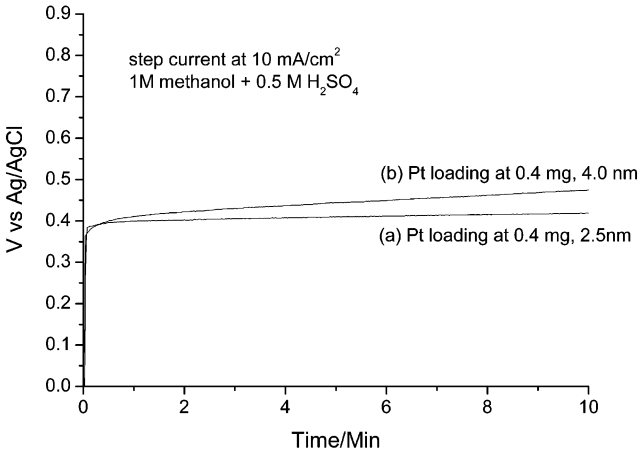

Figure 9. Chronopotentiograms similar to those in Figuer 8 with the same Pt loading but different particle size: (a) Pt loading at 0.2 mg/cm^2, particle size at 2.5 nm prepared by 20 mM H_2PtCl_6 and 20 mM $RuCl_3$ in precursor; (b) Pt loading at 0.4 mg/cm^2, particle size at 4.0 nm prepared by 40 mM H_2PtCl_6 and 40 mM $RuCl_3$ precursor.

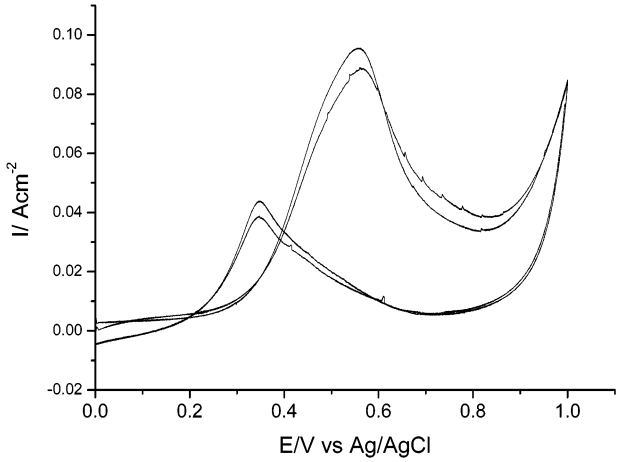

Figure 10. Cyclic voltammograms of the Pt−Ru nanoparticles/carbon electrode in 1 M methanol + 0.5 M H_2SO_4 at room temperature at a scan rate of 25 mv/s. Pt loading at 0.4 mg/cm^2, particle size at 2.5 nm prepared by 20 mM H_2PtCl_6 and 20 mM $RuCl_3$ precursor.

dispersion on the carbon paper, and the high electrocatalytic activity of the Pt−Ru nanoparticles. These results demonstrate the advantage of Pt−Ru binary metal nanoparticles prepared by microemulsion and their potential for direct methanol fuel cell applications. The high catalytic activity and better performance of Pt−Ru alloy catalysts compared to those of a pure Pt catalyst over a wide potential range have been studied and explained by several researchers.[46] The OH_{ad} required for the oxidation of the CO was formed as a reaction intermediate during methanol oxidation at more cathodic potentials due to the high affinity of the Ru surface atoms toward OH formation. The XPS spectra of the Pt−Ru nanoparticles indicated that ruthenium oxide and Pt^0 were the main components of the Pt−Ru nanoparticles. This result suggests that the active oxygen required for CO oxidation is provided at the second metal (Ru) rather than at a Pt site. Ruthenium oxides may serve as the source of oxygen that isrequired for the methanol oxidation reaction.[47]

Conclusions

The synthesis of Pt−Ru nanoparticles has been achieved through reverse microemulsions of water/Triton X-100/propanol-2/cyclohexane (w/o) and the reduction of aqueous Pt−Ru precursor solution with a parallel hydrazine microemulsion system. Below 20 mM of precursor solution, the TEM images indicated an average size of Pt−Ru nanoparticle of 2.5 nm with a narrow size distribution. XRD results show the homogeneous alloy structure of Pt and Ru. The atom ratio of Pt to Ru from EDX and ED analyses is in close agreement with the original precursor concentration. XPS analysis indicated a surface composition of Pt metal and Ru oxides. The composition of bimetallic Pt−Ru nanoparticles can be conveniently controlled by adjusting the initial metal salt solution. The size of Pt−Ru nanoparticles is relationally largest at higher precursor concentration but levels off at 4.6 nm at 100 mM concentration of Pt−Ru precursor solution. From analyses of the microemulsion droplet size, the size of the particles appears to be limited by nucleation at low precursor concentration and limited by collisions with hydrazine droplets at high precursor concentration. The electrochemical experiments showed that the Pt−Ru nanoparticles supported on carbon paper electrode have higher catalytic activity toward methanol oxidation at room temperature.

Acknowledgment. This work was supported by the Research Grants Council of Hong Kong (HKU 7072/019) and HKU Foundation Seed Grant. We thank the Electron Microscope Unit and Dr. J. Gao of the Department of Physics for the use of TEM, EDX, and XRD. We also thank Dr. Alfonso Ngan for helpful discussion of the TEM ED results. The XPS and TEM-EDX results were performed in CUHK.

CM0203868

(46) (a) Watanabe, M.; Motoo, S. *J. Electroanal. Chem.* **1975**, *60*, 275. (b) Iwasita, T.; Nart, F. C.; Vielstich, W. *Ber. Bunsen-Ges. Phys. Chem.* **1990**, *94*, 1030. (c) Gasteiger, H. A.; Markovic, N.; Ross, P. N., Jr.; Cairns, E. J. *J. Phys. Chem.* **1993**, *97*(12), 020. (d) Deborah, L. B.; Cregg, A. D.; Edward, A. K.; William, D. K.; Lukehart, C. M.; *Chem. Mater.* **2001**, *13*, 891.

(47) (a) Watanabe, M.; Uchida, M.; Motoo, S. *J. Electroanal. Chem.* **1987**, *229*, 395. (b) Cooper, S. J.; Gunner, A. G.; Hoogers, G.; Thompsett, D. *Procedings of the 2nd International Symposium on New Materials for Fuel Cells and Modern Battery Systems*; Montreal, 1997. (c) Liu, R.; Iddir, H.; Fan, Q.; Hou, G.; Bo, A.; Ley, K. L.; Smotkin, E. S.; Sung, Y. E.; Thomas, H. K. S.; Wieckowski, A. *J. Phys. Chem. B* **2000**, *104*, 3518.